


ORIGINAL ARTICLE

Proteomic and transcriptomic profiling of *Pten* gene-knockout mouse model of prostate cancer

Jinhui Zhang PhD¹ | Sangyub Kim PhD² | Li Li PhD¹ | Christopher J. Kemp PhD³ |
Cheng Jiang MD^{1,2} | Junxuan Lü PhD^{1,2} 

¹Department of Biomedical Sciences, School of Pharmacy, Texas Tech University Health Sciences Center, Amarillo, Texas

²Department of Pharmacology, Pennsylvania State University College of Medicine, Hershey, Pennsylvania

³Human Biology Division and Public Health Sciences Division, Fred Hutchinson Cancer Research Center, Seattle, Washington

Correspondence

Junxuan Lü, PhD, Department of Pharmacology, Penn State College of Medicine, Hershey, PA 17033.

Email: junxuanlu@pennstatehealth.psu.edu

Present address

Jinhui Zhang and Li Li, Food and Drug Administration, Silver Spring, MD.

Funding information

Penn State College of Medicine Start-up fund; Texas Tech University Health Sciences Center Preliminary Data Grant; National Cancer Institute, Grant/Award Number: R01CA172169

Abstract

Background: The prostate-specific phosphatase and tensin homolog deleted on chromosome 10 (*Pten*) gene-conditional knockout (KO) mouse carcinogenesis model is highly desirable for studies of prostate cancer biology and chemoprevention due to its close resemblance of primary molecular defect and many histopathological features of human prostate cancer including androgen response and disease progression from prostatic intraepithelial neoplasia to invasive adenocarcinoma. Here, we profiled the proteome and transcriptome of the *Pten*-KO mouse prostate tumors for global macromolecular expression alterations for signaling changes and biomarker signatures.

Methods: For proteomics, four pairs of whole prostates from tissue-specific conditional knockout *Pten*-KO mice (12–15 weeks of age) and their respective wild-type littermates housed in the same cages were analyzed by 8-plex isobaric tags for relative and absolute quantitation iTRAQ. For microarray transcriptomic analysis, three additional matched pairs of prostate/tumor specimens from respective mice at 20 to 22 weeks of age were used. Real-time quantitative reverse transcription-polymerase chain reaction was used to verify the trends of protein and RNA expression changes. Gene Set Enrichment Analysis and Ingenuity Pathway Analysis were carried out for bioinformatic characterizations of pathways and networks.

Results: At the macromolecular level, proteomic and transcriptomic analyses complement and cross-validate to reveal overexpression signatures including inflammation and immune alterations, in particular, neutrophil/myeloid lineage suppressor cell features, chromatin/histones, ion and nutrient transporters, and select glutathione peroxidases and transferases in *Pten*-KO prostate tumors. Suppressed expression patterns in the *Pten*-KO prostate tumors included glandular differentiation such as secretory proteins and androgen receptor targets, smooth

Abbreviations: AR, androgen receptor; ER, endoplasmic reticulum; GSEA, Gene Set Enrichment Analysis; HG-PIN, high-grade prostatic intraepithelial neoplasia; IPA, Ingenuity Pathway Analysis; iTRAQ, isobaric tags for relative and absolute quantitation; KO, knockout; mTOR, mammalian target of rapamycin; MDS, multidimensional scaling; NF- κ B, nuclear factor-kappaB gene or protein; Pten/PTEN, phosphatase and tensin homolog deleted on chromosome 10 gene or its encoded protein; PCA, prostate cancer; PICS, PTEN-deficiency induced cellular senescence; qRT-PCR, quantitative or real time reverse transcription-polymerase chain reaction; TRAMP, transgenic adenocarcinoma of mouse prostate; WT, wild type.

Jinhui Zhang and Sangyub Kim contributed equally to this study.

This is an open access article under the terms of the Creative Commons Attribution-NonCommercial License, which permits use, distribution and reproduction in any medium, provided the original work is properly cited and is not used for commercial purposes.

© 2020 The Authors. *The Prostate* published by Wiley Periodicals, Inc.

muscle features, and endoplasmic reticulum stress proteins. Bioinformatic analyses identified *immune and inflammation responses* as the most profound macromolecular landscape changes, and the predicted key nodal activities through Akt, nuclear factor-kappaB, and P53 in the *Pten*-KO prostate tumor. Comparison with other genetically modified mouse prostate carcinogenesis models revealed notable molecular distinctions, especially the dominance of *immune and inflammation features* in the *Pten*-KO prostate tumors.

Conclusions: Our work identified prominent macromolecular signatures and key nodal molecules that help to illuminate the patho- and immunobiology of *Pten*-loss driven prostate cancer and can facilitate the choice of biomarkers for chemoprevention and interception studies in this clinically relevant mouse prostate cancer model.

KEYWORDS

adenocarcinoma, animal model, expression signatures, macromolecular biomarkers, prostate cancer

1 | INTRODUCTION

Prostate cancer (PCa) is the second leading cause of cancer-related death for men in the USA.¹ The phosphatase and tensin homolog deleted on chromosome 10 (PTEN) enzyme, by dephosphorylating the 3' position of phosphatidylinositol-3,4,5-trisphosphate to phosphatidylinositol 4,5-bisphosphate, antagonizes the phosphatidylinositol-3-OH kinase (PI3K)-Protein kinase B (AKT)-mammalian target of rapamycin (mTOR) signaling pathway that stimulates cell metabolism, growth, proliferation, and survival.² *PTEN* loss was identified in up to 45% of high-grade prostatic intraepithelial neoplasia (HG-PIN) lesions²⁻⁴ and up to 70% in advanced PCa.⁵ Our analyses with cBioPortal also showed that *PTEN* genomic alterations (mostly copy number deletion) ranged from 20% to 30% in prostate adenocarcinoma and increased to as high as 70% in metastatic and castration-resistant PCa (Figure S1). In support of a causal role of PTEN loss in the development of PCa, mouse genetic model studies by the Hong Wu laboratory⁶ and subsequently by others have demonstrated that tissue-specific conditional knockout (KO) of *Pten* gene in prostate epithelium rapidly causes HG-PINs that progress to invasive adenocarcinoma. The prostate-specific *Pten*-KO mouse model resembles many histopathological features of human PCa including androgen responsiveness and disease progression. In particular, the preservation of androgen receptor (AR) and P53 tumor suppressor in the early lesions and adenocarcinomas of *Pten*-KO prostate is superior to the more widely used transgenic adenocarcinoma of mouse prostate (TRAMP) model, in which nonepithelial neuroendocrine carcinomas prevail,⁷ to study prostate carcinogenesis and its prevention and therapy.

As many other malignancies, PCa is a complex disease involving multiple abnormalities at the levels of DNA, RNA, proteins, and metabolites. Omics technologies have enabled investigation of the genomic, transcriptomic, proteomic, and metabolomics changes through high-throughput interfaces in a global-unbiased manner.⁸ Previously, other laboratories have reported the microarray-based transcriptome of *Pten*-KO mutant prostate⁶ and glycoprotein proteome of serum and

prostate of *Pten*-KO mutant mice.⁹ However, the different omic platforms have their respective technological limitations. For example, proteomics is biased for the detection of high abundance proteins due to detection sensitivity limitation. Microarray hybridization transcriptomics, on the other hand, may underestimate the expression of a significant proportion of genes (~1/5) due to probe dynamic range. Combining different omics platforms for macromolecular entities will likely provide a more comprehensive credentialing of the molecular changes and a better understanding of the complex biological processes involved in *Pten*-KO mutant prostate carcinogenesis. The obtained data sets could provide “reference” signatures to facilitate the selection of biomarkers for mechanistic interrogations of this model in chemoprevention and therapy studies. In the work reported here, we deployed *isobaric tags for relative and absolute quantitation* (iTRAQ) proteomics and microarray transcriptomics to identify macromolecular changes associated with *Pten*-KO mouse prostate carcinogenesis.

2 | MATERIALS AND METHODS

2.1 | Biospecimens

The mouse tissues were provided by the Mouse Model Repository for Cancer Biomarker Discovery sponsored by National Cancer Institute Mouse Proteomics Initiative (<http://proteomics.cancer.gov/programs/completed/mouseinitiative>).¹⁰ Mice of the *Pten*-KO genotype and their wild-type (WT) littermates in 129 background originated by the Hong Wu laboratory⁶ were housed at the Fred Hutchinson Cancer Research Center from April 2005 to April 2007. When a tumor was palpable, the *Pten*-KO mouse and its WT littermate housed in the same cage were killed on the same day by CO₂ asphyxiation. Tumors from *Pten*-KO mice and whole prostates from litter-/cage-mates were dissected during necropsy, snap frozen, and stored in liquid nitrogen. Eight pairs of prostate/tumor tissue

specimens were shipped to Texas Tech University Health Sciences Center on dry ice (received on 08/02/2011) and then stored at -80°C until analyses.

2.2 | iTRAQ-8 plex proteomics

Four pairs of prostate/tumor (12–15 weeks) were used for proteomic profiling. Proteins were extracted, denatured, reduced, alkylated, and digested to peptides, as previously reported.^{11–13} Peptides were then labeled with 8-plex iTRAQ reagents according to the manufacturer's protocol (Sciex Headquarters, Legal Entity: AB Sciex LLC, Framingham, MA). Labeled peptides were pooled, fractionized using reverse phase chromatography, and analyzed using capillary liquid chromatography coupled with a Velos Orbitrap mass spectrometer (Thermo Fisher Scientific) as reported.¹⁴ ProteinPilot 4.2 (Sciex) software was used for data processing. Data was presented as the relative expression ratio of a given protein in the prostate of *Pten*-KO mice to that of WT litter-/cage-mates. For example, the protein sample of *Pten*-KO mouse was assigned to 114 reporter, and that of its cage-mate WT mouse was prepared with 113 reporter. To call proteins differentially expressed between *Pten*-KO and WT samples, we used the following parameters adapted from a recent report¹⁵: (a) proteins should have been identified with greater than 99% confidence (equivalent to local FDR < 1% and unused scored above 2) and at least one unique peptide; (b) for protein ratio quantitation of each cage-mates pair, *P* value should be lower than .05 for at least one pair; (c) expression ratio change patterns among *Pten*-KO/WT pairs should be concordant in direction; and (d) group mean protein expression ratio cutoff value of > 1.20 or < 0.80, based on our previous work with measurement error consideration.^{11,12} The results of proteomics were further corroborated by real-time quantitative reverse-transcription polymerase chain reaction (RT-PCR) for the corresponding messenger RNA (mRNA) of selected proteins, as previously reported.¹³ Preliminary results were communicated at the American Association for Cancer Research (AACR) annual meeting in 2013 (Zhang et al *Proteomic profiling of Pten-deletion mouse prostate and its molecular pharmacodynamic responses to methylseleninic acid*. Abstract #315).

2.3 | Microarray transcriptomics

Three pairs of prostate/tumor from older mice (at 20–22 weeks of age) than those for the iTRAQ work were used for gene expression analysis. Total RNAs were extracted using RNeasy Mini kit (QIAGEN, Germantown, MD). mRNA expression profiles of individual prostate/tumor were analyzed using Mouse Ref-8 BeadChip expression array (Illumina, Inc, San Diego, CA) as previously described.¹³ All RNA labeling and hybridization were performed at the BioMedical Genomics Center of the University of Minnesota according to protocols specified by the manufacturers. Data filter was set for probe detection *P*-value ($P \leq .05$) and cutoff log₂ fold change ≥ 0.585 or ≤ -0.585

(fold change ≥ 1.5 and ≤ 0.667) between *Pten*-KO and *Pten*-wild type (WT) groups. Two-tailed, paired Student *t* test (parametric) was used to compare the log-transformed expression intensity of each gene between the *Pten*-KO mice and matched litter-/cage-mates. The paired *t* test was most appropriate to control/account for breeding stock, housing/environment, and age variations among the *Pten*-KO and WT mice.

2.4 | Real-time RT-PCR

The results of transcriptomics were further confirmed by real-time quantitative reverse-transcription polymerase chain reaction (qRT-PCR) as previously described¹³ using the Fast Start Universal SYBR Master with ROX (Roche; Millipore-Sigma, St. Louis, MO) with an ABI 7300 Real-Time PCR System (Applied Biosystems, Foster City, CA).¹³ β -actin was selected as the housekeeping gene for normalization. Primers specific for each gene is listed in Table S1.

2.5 | Gene Set Enrichment Analysis of differentially expressed genes and proteins

Gene Set Enrichment Analysis (GSEA) was done by GSEA software v4.0.3, which applies predefined gene sets from the Molecular Signatures Database (MSigDB v7.0). For the present study, we used Gene Ontology (C5) database and oncology database (C6) in MSigDB for GSEA analyses. As previously mentioned, proteomic data were presented as the relative expression ratio of proteins between *Pten*-KO mouse prostate and matched WT litter-/cage-mate prostate. GSEA was conducted using the preranked list according to protein fold changes and 1000 time permutation test. The minimum and maximum criteria for the selection of protein sets from the collection were 5 and 500 proteins, respectively. For transcriptomics, differentially expressed genes were ranked by log₂ ratio of classes and permuted 1000 times to the gene set. The minimum and maximum criteria for the selection of gene sets from the collection were 15 and 500 genes, respectively. Heatmaps were prepared by GSEA software. Multidimensional scaling (MDS) plot was drawn by Degust tool (<http://degust.erc.monash.edu/>).

2.6 | Transcriptomics and proteomics analyses using Ingenuity Pathway Analysis

Each proteomic and transcriptomic data was uploaded to Ingenuity Pathway Analysis (IPA) software (QIAGEN). IPA core analyses were performed to identify important functions, networks, and associations using the following parameter amendments to IPA default criteria adapted from a recent report¹⁶: (a) direct and indirect relationships; (b) generation of interaction networks with 140 genes per network or 35 proteins per network (due to the relatively low number of proteins identified); and (c) species, mouse (with stringent filtering).

The interactions (gene-gene, gene-protein, protein-protein, etc), canonical pathways, upstream regulatory analysis, and functional networks were generated through IPA core analysis. Based on the results from IPA core analyses, networks and their associated diseases and functions were further investigated to interpret biological and molecular changes in *Pten*-KO mouse prostate tumor compared with WT litter-/cage-mate prostate.

2.7 | cBioPortal database analysis

PTEN mutations in PCa patients' data were searched among four different PCa studies on cBioPortal database (Figure S1). The search parameters included copy number alterations (amplification and deep deletion), fusions, mutations, and multiple alterations.

3 | RESULTS

3.1 | Proteome

Our 8-plex iTRAQ proteomic approach identified 711 proteins (Table S2) with local FDR < 1% and at least two unique peptides per protein (FDR summary data are provided in Table S3). This number was higher than the 563 proteins identified by Cima et al⁹ using a label-free liquid chromatography-mass spectrometry approach for enriched glycoproteins from the *Pten*-KO prostate. The list was narrowed to 104 proteins which met the four criteria described in Methods section for differential protein abundance between *Pten*-KO mutant and WT prostate. Among them, 55 proteins were overexpressed by 20% or more and 49 proteins were downregulated by 20% or more in *Pten*-KO mutant prostate relative to WT prostate (Table S4).

Seventeen proteins exceeded two-fold overexpression (average of match pair ratios 2.2×:18.5×) in the *Pten*-KO prostate relative to WT glands (Table 1). Literature searches indicated that 14 of the top 25 proteins overexpressed in *Pten*-KO mouse prostate were associated with inflammation and/or immunity. Specifically, myeloid/neutrophil-related innate immunity marker S100a8/calprotectin and Ltf/lactotransferrin (another myeloid lineage marker tracking neutrophils, monocytes/macrophages, and distinct subtypes of dendritic cells¹⁷) stood out along with Reg3g, Pglyrp1, Lgals3, Pigr, Lcn2, Anxa1, Anxa3, and so forth. Other changes included glutathione conjugative metabolism (Gsto1 and Gsta4), proteases related to invasiveness, histones, and chromatin features related to enhanced cell proliferation.

Based on the 56 upregulated proteins, preranked GSEA for protein enrichment analysis indicated significant changes in immune and inflammation responses (Figure 1A and Table S5). IPA network analysis of the upregulated proteins revealed *cancer*, *inflammatory response*, and *organismal injury and abnormalities* to be the most significantly enriched ($P = .0483$ - $6.65E-09$) (Figure 1C). IPA network analysis predicted nuclear factor-kappaB (NF-κB) as a key central hub in the top network to interact directly with MMP9, while indirectly with S100A8, CLU, IL24, and so forth (Figure 1C). Not

surprisingly, NF-κB signaling is best known for inflammation and immune responses. Therefore, the top protein abundance increases in the *Pten*-KO mouse prostate tumors implicated landscape changes for the *inflammation and immune systems*. The overexpression of histone and chromatin features was consistent with the increased proliferation of the *Pten*-KO epithelial lesions.

Among the downregulated proteins in *Pten*-KO prostate, five proteins (Defb50, Tgm4, C1rb, Pbsn, and Msmb) displayed greater than a five-fold reduction in comparison with the matched WT litter-/cage-mate (KO/WT ratio from 0.07 to 0.18) (Table 1). These five proteins were related to *prostate gland differentiation and secretory functions* including prostate secretions and AR target proteins. Two other notable features of the decreased protein abundances related to *endoplasmic reticulum (ER) stress regulators* and *smooth muscle* proteins in the *Pten*-KO prostate (Table 1). The latter feature could result from a faster expanding neoplastic epithelium compartment out-pacing the smooth muscle cells in the mutant prostate, leading to a "shrinking" proportional metric.

Based on the 49 downregulated proteins (eg, Apoa1, Fkbp2, Hsp9b1, etc), preranked GSEA for protein enrichment analysis suggested *ER stress response* (Figure 1B and Table S5). IPA network analysis showed *oxidative stress* and *molecular transport* the most significant pathways ($P = .035$ - $8.92E-11$) (Figure 1D). P53 protein function was weakly implicated through networking directly with SOD1, PPARA, AKR1B7, AKR1B1, and so forth (Figure 1D).

All predicted activating upstream regulators, including IL4, NFE2L2, HNF1A, and IL6, were associated with *inflammatory response*, whereas the predicted inhibitory upstream regulators P53, SRF, and RICTOR were associated with *response to oxidative stress*. An inflammatory cytokine IL5 was weakly predicted as another inhibitory upstream regulator (Table S6).

3.2 | Comparison with existing proteomic data sets

Five proteins (Lgals3, Pigr, Ltf, Cfb, and Clu) among the top 25 upregulated proteins identified in the present work matched the earlier proteomic data set of Cima et al⁹ (Table 1). Similarly, among the top 25 downregulated proteins detected by our iTRAQ approach, eight were detected by Cima et al⁹ (Table 1). The discrepancy was probably due to their technical bias for detection of glycoproteins for serum-based proteomic biomarkers of PCa.⁹

A comparison of *Pten*-KO with the TRAMP model revealed that 44% (22/50) of top 50 proteins displayed concordant directions of change in both models. Most of the downregulated proteins in the *Pten*-KO prostate were also decreased in the TRAMP mutant prostate (Table 1). These concordant changes in both models suggested that such proteins might play common roles in prostate carcinogenesis, or the changes could be an indication of the disruption of normal prostate function or alteration of the proportion of the different cellular types. However, some of the upregulated proteins in *Pten*-KO mutant prostate/tumor were not changed (eg, S100a8 and Cfb) or even decreased (eg, Lcn2 and Wfdc2) in the TRAMP mutant prostate/tumor (Table 1). These discordant proteins were related to neutrophil/myeloid lineage

TABLE 1 Top 50 proteomic changes in Pten-KO mouse prostate tumors

Protein	Pten-KO/WT average pair ratio	Function category	Pten-KO/WT glycoproteome	Expression changes detected at mRNA level by		
				Pten-KO/WT (our data set)	Pten-KO/WT (Wu lab)	TRAMP (our data set)
Upregulated proteins (top 25)						
Protein S100-A8 (S100a8) = calprotectin	18.5	Inflammation, innate immunity, and neutrophil	x	Up		No Δ
Regenerating islet-derived protein 3-gamma (Reg3g)	8.32	Inflammation, innate immunity, and stem cell	x	UP	N/A	
Galectin-3 (Lgals3)	6.23	Inflammation and immunity	Up	Up		Up
Lipocalin (Lcn2), neutrophil gelatinase-associated = NGAL, oncogene 24p3	4.14	Immunity, Inflammation, and neutrophil	x	Up	N/A	Down
Chitinase-3-like protein 3 (Chi3l3) = ym1	4.52	Inflammation and macrophage secretion	x		N/A	Up
Peptidoglycan recognition protein 1 (Pglyrp1) = Tag7	6.85	Immunity, neutrophil, and bactericidal	x	Up		
Polymeric immunoglobulin receptor (Pigr)	5.5	Immunity, adaptive IgM, and IgA	Up	Up		Up
Cathelin-related antimicrobial peptide (Camp)	5.82	Immunity	x	Up		
Lactotransferrin (Ltf)	3.00	Immunity, myeloid marker, neutrophil, and macrophages	Up	Up		
Complement factor B (Cfb)	1.89	Immunity	Up	Up		No Δ
Calcium-activated chloride channel regulator 1 (Clca1)	3.78	Inflammation	x		Up	
Proteasome activator complex subunit 1 (Psme1)	1.71	Immunity and adaptive	x	Up		
Annexin A1 (Anxa1)	2.5	Inflammation, anti-; innate immunity and neutrophil	x	Up	Up	
Annexin A3 (Anxa3)	2.26	Inflammation, anti-; innate immunity and neutrophil	x	Up	Up	
Clusterin (Clu) = testosterone-repressed prostate message-2 (TRPM-2)	4.03	Oncogene, antiapoptotic; heat shock protein	Up	UP		Up
Glutathione S-transferase omega-1 (Gsto1)	2.99	Drug metabolism, phase II	x	Up	Up	
Glutathione S-transferase A4 (Gsta4)	1.98	Drug metabolism, phase II	x			
Glutathione disulfide reductase, mitochondrial (GSR)	1.98	Cell redox homeostasis	x			
Carbonyl reductase (NADPH) 2 (Cbr2) = adipocyte protein 27	1.73	Drug metabolism, mitochondria alkyl dehydrogenase	x	Up	Up	

TABLE 1 (Continued)

Protein	Pten-KO/WT average pair ratio	Function category	Pten-KO/WT glycoproteome	Expression changes detected at mRNA level by	
				Pten-KO/WT (our data set)	Pten-KO/WT (Wu lab) data set
WAP four-disulfide core domain protein 2 (Wfdc2) = human epididymis protein 4 (HE4)	4.49	Protease inhibitor; fibrosis	x	Up	Down
Matrilysin (Mmp7)	2.21	Proteases; invasion	x		
60S ribosomal protein L13 (Rp13)	1.98	Protein synthesis	x		
Heterogeneous nuclear ribonucleoprotein U (Hnrnpu)	1.77	Chromatin	x		
Histone H3.3 (H3f3a)	1.72	Chromatin	x	Up	Up
Histone H4 (Hist1h4a)	1.96	Chromatin	x		Up
Downregulated proteins (top 25)					
Beta-defensin50 (Defb50)	0.07	Prostate secretion; immune defense	Down		Down
Protein-glutamine gamma-glutamyltransferase 4 (Tgm4) = transglutaminase 4	0.11	Prostate secretion, AR target	x	Down	Down
Beta-microseminoprotein (Msb) = prostatic secretory protein 94 (PSP94)	0.18	Prostate secretion	Down		Down
Complement C1r-B subcomponent (C1rb)	0.17	Prostate-specific serine protease; immunity	x	Down	Down
Probasin (Pbsn)	0.17	Prostate-specific, AR target	Down	N/A	Down
Peroxioredoxin-6 (Prdx6)	0.32	Prostate secretion	Down		Down
Prostate and testis expressed protein 4 (Pate4)	0.58	Prostate secretion	x		Down
Serine protease inhibitor kazal-like protein, minor form (Spink)	0.65	Prostate secretion	x		
Cysteine and glycine-rich protein 1 (Csrp1)	0.63	Prostate secretion	x	Down	Down
Cysteine-rich secretory protein 1 (Crisp1)	0.64	Prostate secretion	x		Down
Protein disulfide-isomerase A6 (Pdia6)	0.42	ER stress regulator	x		Down
Protein disulfide-isomerase A4 (Pdia4)	0.42	ER stress regulator	Down		Down
Protein disulfide-isomerase A3 (Pdia3)	0.63	ER stress regulator	x		Down
Endoplasmic = heat shock protein 90B1 (Hsp90b1)	0.49	ER stress regulator	Down		Down
78 kDa glucose-regulated protein (Grp78) = Heat shock 70-kDa protein 5 (Hspa5)	0.51	ER stress regulator	Down		Down

(Continues)

TABLE 1 (Continued)

Protein	Pten-KO/WT average pair ratio	Function category	Pten-KO/WT glycoproteome	Expression changes detected at mRNA level by microarray and/or qRT-PCR	
				Pten-KO/WT (our data set)	Pten-KO/WT (Wu lab)
Aldose reductase-related protein 1 (Akr1b7)	0.61	ER stress regulator	x	Down	
Peptidyl-prolyl cis-trans isomerase FKBP2 (Fkbp2)	0.64	ER stress regulator	x		
Mesencephalic astrocyte-derived neurotrophic factor (Manf)	0.60	ER stress regulator; lipid binding	x		
Isoform fibroblast of tropomyosin alpha-1 chain (Tpm1)	0.57	Muscle	x	Down	Down
Isoform TM-1 of Tropomyosin beta chain (Tpm2)	0.59	Muscle	x	Down	Down
Calponin-1 (Cnn1)	0.62	Muscle	x	Down	Down
Transgelin (Tagln)	0.65	Muscle	Down	Down	Down
Actin, aortic smooth muscle (Acta2)	0.65	Muscle	x		
Hemoglobin subunit beta-1 (Hbb-b1)	0.65	Erythrocyte, oxygen binding	x		
Hemoglobin subunit beta-2 (Hbb-b2)	0.57	Erythrocyte, oxygen binding	x		

Abbreviations: AR, androgen receptor; mRNA, messenger RNA; N/A, nonavailability; Pten-KO, phosphatase and tensin homolog deleted on chromosome 10-knockout; qRT-PCR, real-time quantitative reverse-transcription polymerase chain reaction; TRAMP, transgenic adenocarcinoma of mouse prostate; WT, wild type.

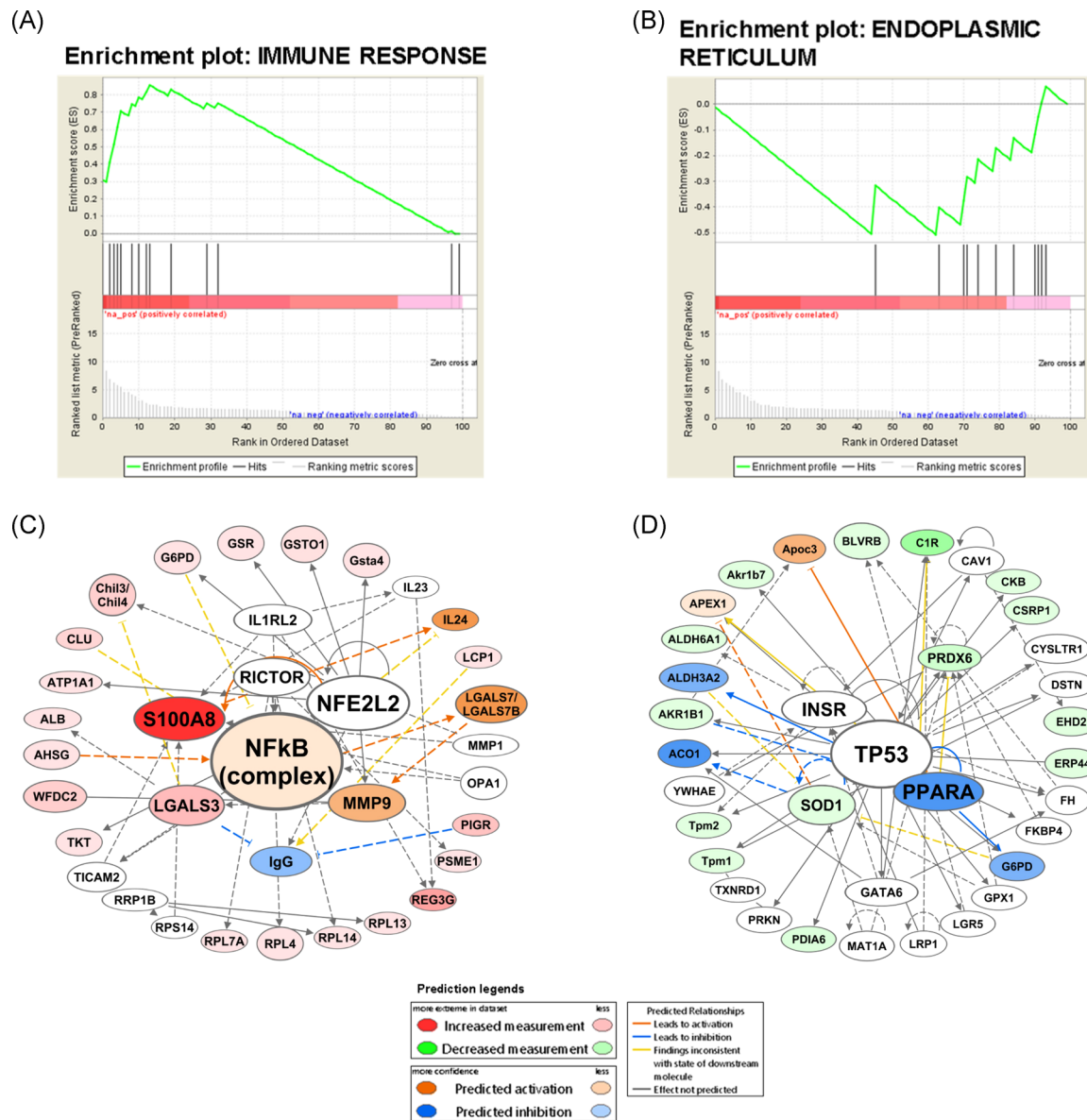


FIGURE 1 Proteomic data analyses. Enrichment of proteins in (A) immune response ($P < .0001$) increased in, and (B) endoplasmic reticulum ($P < .0001$) decreased in PTEN-KO mouse prostate compared with WT by using preranked GSEA. C, IPA network analysis displaying interactions among upregulated proteins related to cancer, inflammatory response, and organismal injury and abnormalities ($P = .0483$ – $6.65E-09$). D, IPA network analysis displaying interactions among downregulated proteins related to oxidative stress and molecular transport ($P = .035$ – $8.92E-11$). P53 involvement was equivocally implicated. GSEA, Gene Set Enrichment Analysis; IPA, Ingenuity Pathway Analysis; NF- κ B, nuclear factor- κ B; PTEN-KO, phosphatase and tensin homolog deleted on chromosome 10-knockout; WT, wild type

immune cell features. These latter observations highlighted also unique molecular, in particular, immunological, differences of the two mouse models of prostate carcinogenesis.

3.3 | Limitations of iTRAQ proteomics

Common to nonantibody-based proteomic approaches, a major limitation of iTRAQ proteomics is bias for the detection of high abundance proteins due to the detection sensitivity issue. Therefore, signaling proteins, such as immune or inflammatory cytokines and

chemokines, usually expressed at a low level would present more technical challenges to proteomics than structural proteins that make up the tumor tissue architecture (Table S2). In addition, it was challenging for technology to detect posttranslational protein modifications that could significantly regulate protein functional activity. Furthermore, it has been well established that mutant epithelial lesion progression in *Pten*-KO model is constrained by a special type of cellular senescence called PTEN-deficiency-induced cellular senescence (PICS).¹⁸ Studies have shown that PICS is mediated by P53 protein stabilization and elevation of its canonical target P21Cip1 (*Cdkn1a*).^{19,20} However, we failed to detect P53 or P21Cip1 proteins

by iTRAQ signals in the *Pten*-KO prostate. Moreover, the small number of proteins failed to predict AKT/mTOR activation resulting from the *Pten* deletion and instead predicted inhibited status for P53 and mTOR downstream target RICTOR (Figure 1; Table S6). We, therefore, used a microarray hybridization platform next to interrogate the transcriptomic differences between *Pten*-KO mutant prostate tumors and matched WT prostate from litter/cage mates.

3.4 | Transcriptome

Three cage-/litter-mate pairs of prostate tissue/tumor from older mice (20–22 weeks) than those used for the proteomics analysis were used for the transcriptomic analysis. A total of 423 genes were identified with cutoff threshold set as $P < .05$ and an absolute log2 fold change cutoff ≥ 0.585 over WT (Table S7). Multidimensional scaling (MDS) plot of genes demonstrated that WT prostates were clearly separated from the *Pten*-KO prostate tumors on the global transcriptome expression profiles (Figure 2A). The three mutant glands displayed greater variance than did the three WT glands on MDS dimension 2.

As expected of *Pten* gene deletion to activate AKT and downstream signaling, GSEA indicated enriched AKT pathway components and activation (eg, *Gpx2*, *Tmprss4*, etc) ($P < .005$) in *Pten*-KO prostate tumors (Figure 2B). GSEA suggested also a strong involvement of *defense response to other organism* (eg, *Ltf*, *Il33*, *Irf7*, etc) (Figure 2C), which involved immunological and inflammation pathways. IPA network analysis also showed *cellular growth and proliferation*, *immunological disease*, and *inflammatory response* to be among the most significantly enriched ($P = .0473$ – $2.20E-32$). Consistent with proteomics, IPA network analysis predicted *Nfkb* as a key central hub in the top network to interact directly with *Tlr2*, *Icam1*, 26S proteasome, and so forth, while indirectly with *Egfr*, *Akt*, *Pi3k*, *Il33*, and so forth (Figure 2E). The transcriptome data predicted *Akt* as the second central hub, superior to the proteomic prediction outcome (Figure 1).

The top 50 overexpressed genes by expression ratio between *Pten*-KO prostate tumors and WT prostates were highlighted in Table 2. They included genes coding for most of the proteins identified by our iTRAQ proteomics, such as *Ltf*, *Pglyrp1*, *Lgals3*, *Pigr*, *Wfdc2*, *Anxa3*, *Gsto1*, and so forth. As expected, the microarray detected many more entities than did iTRAQ proteomics, especially for cytokines and chemokines including *Cxcl15*, *Cxcl17*, and *Il33*, and immune cell surface markers including *Cd14* (human analog of murine macrophage/monocyte), myeloid lineage markers *Ly6a* (also known as *stem cell antigen-1*, *Sca-1*), *Ly6c*, and *Ly6e*, the T cell immunosuppressive enzyme *Arg-1* (L-arginase-1) expressed predominantly by myeloid-derived suppressor cells (MDSC), and interferon-gamma-inducible factors *Isg15* and *Ifitm3*. Consistent with and extending upon the iTRAQ proteomics outcome, literature search revealed that half of the top 50 upregulated genes in *Pten*-KO prostate tumors were associated with immunity and/or inflammation. These transcriptomic features plus the proteomic overexpression

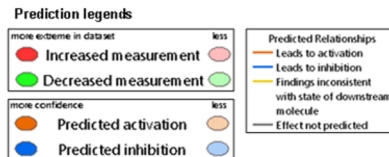
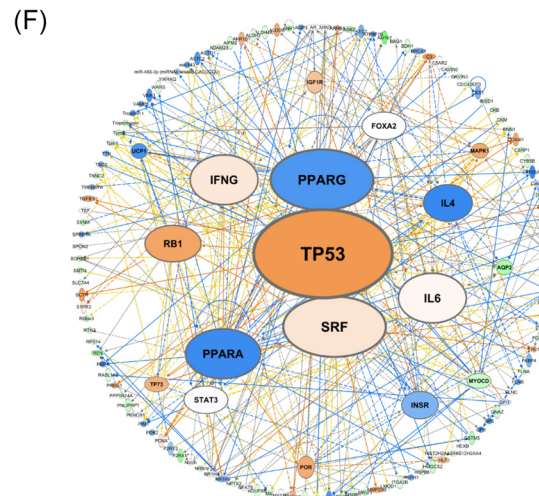
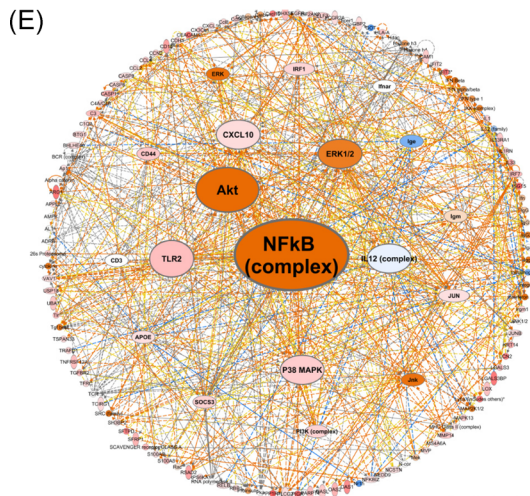
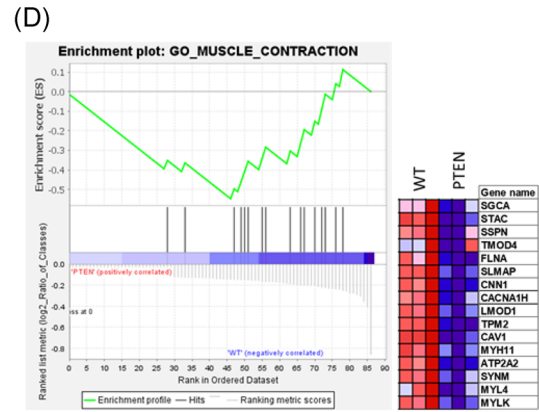
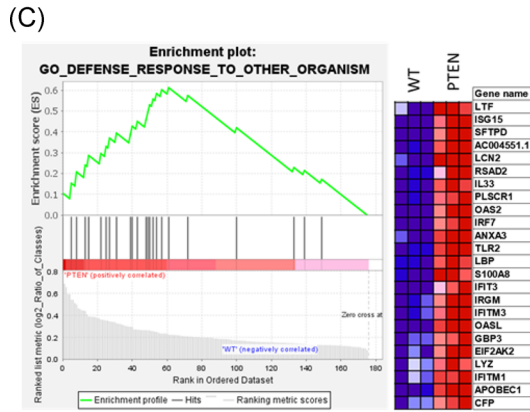
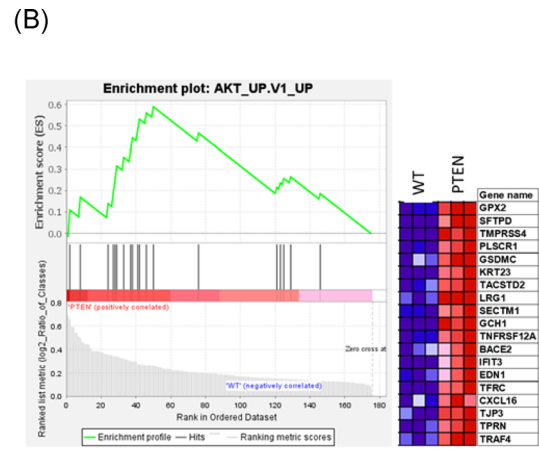
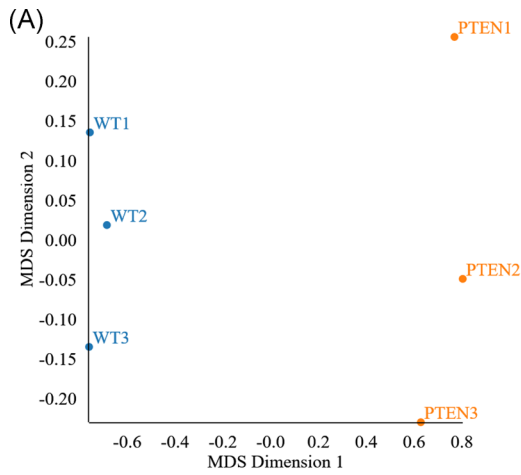
patterns corroborated the observed organ-localized endogenous expansion within the *Pten*-KO prostate tumors of Gr-1+CD11b+ MDSC, neutrophils, and other myeloid lineage monocytes reported by the Hong Wu laboratory²¹ and confirmed by others.^{22,23}

Among the top 50 downregulated genes in *Pten*-KO prostate, near half were related to the *prostate differentiation functions* or the *muscle features* (Table 2). These features corroborated and extended the iTRAQ proteomics in scope and gene entities. GSEA pointed to alterations in *muscle contraction* feature (eg, *Mylk*, *Myl4*, *Myh11*, etc) (Figure 2D). IPA network analysis also revealed *skeletal muscular system development and function*, *molecular transport*, and *organismal development* as the most significant pathways ($P = .0291$ – $4.12E-17$) (Figure 2F). Network analysis of the downregulated proteins predicted P53 gene (*Tp53*) as a key central hub molecule, networking directly with *Aldh4a1*, *Aifm2*, *Cdc42ep3*, *Gstm5*, *Myocd*, and so forth, and indirectly with *Aqp2*, *Itga2b*, *Irfng*, and *Il4* (Figure 2F). As previously mentioned, PICS should involve P53-P21Cip1 signaling to restrain prostate intraepithelial neoplasia (PIN) progression¹⁸ in the absence of DNA damage and repair responses.²⁴ Indeed, several moderately upregulated genes included P53 direct effectors (genes: *Foxa1*, *Casp1*, *Egfr*, *Casp6*, *Cx3cl1*, *Jun*, and *Pml*) and cellular senescence (genes: *Lmnb1*, *Ets2*, *Hist1h2aa*, *Hist1h2ag*, *Hist1h2ah*, *Hist1h2aj*, *Hist1h2am*, *Hist1h2ap*, *Jun*, and *Rps6ka1*). Particularly, IPA network analysis predicted TP53 functions to be upregulated in the *Pten*-KO prostate (Figure 2F), despite a lack of detectable change of *Tp53* mRNA itself.

The predicted activating upstream regulators, such as *Irfng*, *Irfnar*, *Stat1*, and *Tlr3* were associated with *immune response*, whereas *Trim24* and *Sirt1* were predicted inhibitory upstream regulators in association with *skeletal muscle function*. Other predicted inhibitory upstream regulators *Pnpt1* and *Ptger4* were involved in *molecular transport* (Table S8).

3.5 | Comparison with existing microarray data set of *Pten*-KO mutant mouse prostate tumors

Mining the transcriptomic data set from the Hong Wu laboratory,⁶ we found that 54 genes out of 617 (8.8%) in the *Pten*-KO prostate tumors of their older mice (29 weeks of age) showed concordant expression change patterns to our data set (Table S9). In spite of the 7 to 9 weeks age difference for the *Pten*-KO prostate tumor specimens profiled by the two laboratories and only a minor proportion of concordant genes, IPA identified similar top five biological functions, such as *neuroinflammation signaling pathway*, *production of nitric oxide and reactive oxygen species (ROS) in macrophages*, *dendritic cell maturation*, *IL-8 signaling*, and *interferon signaling*, all of which were related to some aspects of inflammation and immunity (Figure S2). As expected, our microarray data set matched with more top 25 up- and 25 downregulated proteins identified by the contemporaneous iTRAQ proteomics than did the Hong Wu laboratory microarray data set performed more than a decade ago (Table 1). The compositional differences for the probe sets on the microarray platforms used by us



and the Hong Wu laboratory could be one reason for the discrepancy.

3.6 | Comparison of *Pten*-KO vs Hi-MYC mutant mouse prostate transcriptomic signatures

Comparing our *Pten*-KO transcriptomic data with the Hi-MYC transgenic mouse prostate data set of the Charles Sawyers laboratory,²⁵ we found that only 3.5% (46 genes out of 1311) showed concordant expression change patterns between both data sets (Table S10). We found distinct sets of gene changes in the mutant prostate of each genetically modified mouse cancer model. Of the top five biological functions, they shared *interferon signaling* as a common feature but differed on *UVA-induced MAPK signaling*. The *Pten*-KO model dominated the three other IPA identified biological functions, *neuroinflammation signaling pathway*, *production of nitric oxide and ROS in macrophages*, and *systemic lupus erythematosus in B cell signaling pathway*, all of which were related to some aspects of inflammation and immunity (Figure S3). The transcriptome comparison between the murine models highlighted that different onco-drivers resulted in distinct molecular signatures in the respective prostate carcinogenesis model.

3.7 | Validation of differential expression of selected genes and proteins by qRT-PCR

Given the biases and limitations of the iTRAQ proteomic and microarray transcriptomic platforms, qRT-PCR was performed to verify mRNA abundance of selected genes/proteins, based on a number of considerations (Figure 3). They included the magnitude of differential expression changes on iTRAQ or microarray detection (eg, *Gapdh*, *Idh1*, and *Ldha* for minimal changes vs *S100A8*, *Reg3g*, *Msmb*, and *Pbsn* for substantial changes); biological functions of interest (eg, *Gapdh*, *Idh1*, and *Ldha* for cellular energetics; *Foxa1*, *Reg3g*, and *CD44* for stem cells; *Nkx3.1* and *Pbsn* for AR targets; *P21Cip1* (*Cdkn1a*) and *Chi3l3* for senescence or aging). The signal for each gene was normalized against that of β -actin as the housekeeping gene. In each case, qRT-PCR was able to confirm the direction of gene expression changes, regardless of whether microarray or iTRAQ was able to detect an entity of interest or not (Figure 3). In general, a substantial

proportion of the microarray hybridization probes underperformed qRT-PCR for estimating the extent of mRNA change (eg, *Cdkn1a/p21*, *Cd44*, *S100A8*, and *Reg3g*) or failed to detect any signal (likely due to missing probes [*Chi3l3* and *Pbsn*]). The expression of *Gapdh* (another commonly used housekeeping gene) and *Ldha* were increased moderately in the *Pten*-KO prostate tumors (Figure 3), consistent with enhanced cellular energy metabolism of the malignant cells.

4 | DISCUSSION

Our analyses of macromolecular expression alterations in *Pten*-KO mouse prostate tumors by iTRAQ proteomics and microarray probe hybridization platforms contribute to and expand the reference mouse omic data sets. In the *Pten*-KO prostate cancer model maintained in the breeding colony at the Fred Hutchinson Cancer Research Center (originated from the Hong Wu Lab), palpable tumors at 12 to 15 weeks (used for proteomics) and 20 to 22 weeks (used for microarray) would represent early to late-stage invasive adenocarcinomas.⁶ Without further dissection or enrichment, the analyzed tissue samples contained many cell types and the extracellular matrix that made up the whole organ/tumor. Therefore, the macromolecular expression changes so obtained would reflect the overall alterations in the whole organ/tumor, without delineation of the specific cell types of origins. The omic data sets should be appreciated and interpreted with such caveats.

Oncogenic phenotypes of PTEN loss have been mostly attributed to AKT activation.²⁶ Consistent with this, our analysis of the transcriptomic data showed that *Pten*-KO in the mouse prostate epithelium led to an enrichment of upregulated genes associated with the AKT pathway activation (Figure 2B) and predicted *Akt* as a central hub gene (Figure 2E). However, the proteomic approach failed this prediction due to the small number of proteins meeting our analysis criteria. Similarly, the transcriptomic data set predicted P53 activation (Figure 2F), whereas the proteomic approach only implicated an inhibitory weak involvement if at all (Figure 1D; Table S6). The progression of PIN lesions in the *Pten*-KO model has been known to be constrained by PICS.¹⁸ *Pten* loss has been shown to trigger PICS through a P53-dependent pathway in mouse prostate tumorigenesis¹⁸ and other cell models,^{2,24} through mTORC1 and mTORC2 driven P53 protein stabilization. Since palpable tumors were collected and analyzed in our work, PICS might have been attenuated to allow the tumors to

FIGURE 2 Transcriptomic analyses of *Pten*-KO prostate tumors vs wild-type (WT) prostate tissue using a statistical approach, GSEA, and IPA. A, Multidimensional scaling (MDS) plot clustering of prostate samples with the three biological replicates of WT (blue) mice and three biological replicates of *Pten*-KO mice (orange). B-D, Enrichment of genes and heatmap of core enrichment genes in (B) Akt Up.V1 Up ($P < .005$) and (C) GO_Defense response to other organism ($P < .005$) by GSEA upregulated in *Pten*-KO as well as (D) GO_Muscle contraction ($P < .05$) by GSEA downregulated in *Pten*-KO tumors. For the heatmaps, columns represent each biological replicate, and rows represent individual genes. The more abundant genes in *Pten*-KO appeared red, and the less abundant genes were colored in blue. E, IPA network analysis displaying interactions among upregulated genes related to *cellular growth and proliferation*, *immunological disease*, and *inflammatory response* ($P = .0473$ - $2.20E-32$). F, IPA network analysis displaying interactions among downregulated genes related to *skeletal muscular system development and function*, *molecular transport*, and *organismal development* ($P = .0291$ - $4.12E-17$). GO, Gene Ontology; GSEA, Gene Set Enrichment Analysis; IPA, Ingenuity Pathway Analysis; PTEN-KO, phosphatase and tensin homolog deleted on chromosome 10-knockout

TABLE 2 Top 100 genes significantly upregulated or downregulated in Pten-KO prostate tumors

Genes	Definition	Pten-KO/WT (Log2 FC)	Pten-KO/WT (FC)	Function category
Upregulated genes (top 50)				
<i>Ltf</i>	Lactotransferrin	5.6	48.50	Immunity, myeloid lineage marker, neutrophil, macrophage, monocyte, and DC subset
<i>Ly6a</i>	Lymphocyte antigen 6 complex, locus A	3.00	8.00	Immunity, myeloid lineage marker, and neutrophil
<i>Ly6c1</i>	Lymphocyte antigen 6 complex, locus C1	2.69	6.45	Immunity, myeloid lineage marker, and neutrophil
<i>Ly6e</i>	Lymphocyte antigen 6 complex, locus E	2.20	4.59	Immunity, myeloid lineage marker, and neutrophil
<i>Arg1</i>	Arginase 1, liver	3.08	8.46	Immunity, myeloid-derived suppressor cells, T cell suppression, and Pten-suppressable
<i>Cd14</i>	CD14 antigen	2.10	4.29	Immunity, myeloid lineage marker, macrophage, and monocyte
<i>Pglyrp1 (Tag7)</i>	Peptidoglycan recognition protein 1	4.6	24.25	Immunity, neutrophil, and bactericidal
<i>Il33</i>	Interleukin 33	1.95	3.86	Immunity and inflammation
<i>Cxcl17</i>	Chemokine (C-X-C motif) ligand 17	4.1	17.15	Inflammation
<i>Cxcl15</i>	Chemokine (C-X-C motif) ligand 15	2.88	7.36	Inflammation
<i>Isg15</i>	ISG15 ubiquitin-like modifier = interferon-simulated gene 15	3.4	10.56	Immunity and innate
<i>Iffit3</i>	Interferon-induced protein with tetratricopeptide repeats 3	3.04	8.22	Inflammation
<i>Iffitm3</i>	Interferon-induced transmembrane protein 3	1.91	3.76	Inflammation
<i>Pigr</i>	Polymeric immunoglobulin receptor	3.28	9.71	Immunity, adaptive IgM, and IgA
<i>Lgals3bp</i>	Lectin galactoside-binding soluble 3-binding protein, galactin-3	2.99	7.94	Immunity and inflammation
<i>Lcn2</i>	Lipocalin 2 = neutrophil-associated lipocalin (NGAL)	2.86	7.26	Inflammation and immunity
<i>Sftpd</i>	Surfactant associated protein D	2.75	6.73	Immunity and innate
<i>Oasl2</i>	2'-5' oligoadenylate synthetase-like 2	2.63	6.19	Immunity, innate, and interferon-activated
<i>Oasl3</i>	2'-5' oligoadenylate synthetase 1G	2.55	5.86	Immunity, innate, and interferon-activated
<i>B4galnt2</i>	Beta-1,4-N-acetyl-galactosaminyl transferase 2	2.23	4.69	Immunity and antigen glycolation
<i>Ubd</i>	Ubiquitin D = IFN γ - and TNF- α -inducible ubiquitin-like modifier FAT10	2.13	4.38	Immunity, innate, antibacterial, and ubiquitin
<i>Rsad2</i>	Radical S-adenosyl methionine domain containing 2 = viperin	2.04	4.11	Immunity, interferon-induced, and antiviral
<i>Noxo1</i>	NADPH oxidase organizer 1	2.95	7.73	Inflammation and superoxide
<i>Anxa3</i>	Annexin A3	2.17	4.50	Inflammation, anti-; innate immunity, and neutrophil
<i>Ppp1r1b</i>	Protein phosphatase 1, regulatory (inhibitor) subunit 1B	3.6	12.13	Oncogene-like, invasion, and angiogenesis

(Continues)

TABLE 2 (Continued)

Genes	Definition	Pten-KO/WT (Log2 FC)	Pten-KO/WT (FC)	Function category
<i>Nupr1</i>	Nuclear protein 1	3.12	8.69	Oncogene and chromatin remodeling
<i>Ckmt1</i>	Creatine kinase, mitochondrial 1, ubiquitous	2.42	5.35	Oncogene-like and metabolism
<i>Tacstd2</i>	Tumor-associated calcium signal transducer 2 = trophoblast (surface antigen)-2 (Trop-2)	2.17	4.50	Oncogene-like and stem cell
<i>Tmprss4</i>	Transmembrane protease, serine 4	3.60	12.13	Protease and invasion
<i>Lrg1</i>	Leucine-rich alpha-2-glycoprotein 1	2.11	4.32	Angiogenesis and binds endoglin
<i>Plscr1</i>	Phospholipid scramblase 1	1.98	3.94	Invasion and metastasis and interferon-induced
<i>Gabbr</i>	Gamma-aminobutyric acid (GABA-A) receptor, pi	1.86	3.63	Invasion motility and basal-like breast cancer
<i>Slc39a4</i>	Solute carrier family 39 (zinc transporter), member 4	4.3	19.70	Transporter, Zn, Stat3, and CREB
<i>Slc40a1</i>	Solute carrier family 40 (iron-regulated transporter), member 1	2.79	6.92	Transporter and Fe recycle macrophage
<i>Slc45a3</i>	Solute carrier family 45 (iron-regulated transporter), member 1 = prostate cancer-associated protein 6 or prostein	2.02	4.06	Transporter and sucrose
<i>Car2</i>	Carbonic anhydrase 2	2.34	5.06	Transporter and CO ₂ acid base homeostasis
<i>Clc6</i>	Chloride intracellular channel 6	1.93	3.81	Transporter and chloride
<i>Clca3</i>	Chloride channel calcium-activated 3	2.50	5.66	Transporter, chloride, and immunity
<i>Cyp2f2</i>	Cytochrome P450, family 2, subfamily f, polypeptide 2	3.8	13.93	Drug metabolism and phase I
<i>Chr2</i>	Carbonyl reductase 2 (NADPH) = adipocyte protein 27	2.85	7.21	Drug metabolism, mitochondria, and dehydrogenase
<i>Gsto1</i>	Glutathione S-transferase omega 1	2.49	5.62	Drug metabolism and phase II
<i>Ceacam1</i>	Carcinoembryonic antigen-related cell adhesion molecule 1	3.10	8.57	Epithelial surface protein
<i>Galm1</i>	Golgi membrane protein 1	2.29	4.89	Epithelial marker and prostate
<i>Gsdmc2</i> (LOC100045250)	Gasdermin C2	1.94	3.84	Epithelial marker
<i>Krt17</i>	Keratin 17	2.17	4.50	Epithelial (type I) cytokeratin
<i>Krt23</i>	Keratin 23	1.92	3.78	Epithelial (type I), cytokeratin
<i>Wfdc18/Expi</i>	WAP four-disulfide core domain 18 (wfdc18) = extracellular proteinase inhibitor (Expi)	3.9	14.93	Fibrosis and protease inhibitor
<i>Wfdc2</i>	WAP four-disulfide core domain 2 = human epididymis protein 4 (HE4)	2.76	6.77	Fibrosis and protease inhibitor
<i>Gpx2</i>	Glutathione peroxidase 2	4.2	18.38	Antioxidation and selenium-dependent
<i>Urah</i>	Urate (5-hydroxyiso-) hydrolase	2.28	4.86	Purine metabolism

TABLE 2 (Continued)

Genes	Definition	Pten-KO/WT (Log ₂ FC)	Pten-KO/WT (FC)	Function category
Downregulated genes (top 50)				
<i>P2rx1</i>	Purinergic receptor P2X ₁ ligand-gated ion channel, 1	-2.41	0.19	Muscle and contraction
<i>Mylk</i>	Myosin, light polypeptide kinase	-2.12	0.23	Muscle
<i>Pdlim3</i>	PDZ and LIM domain 3	-1.75	0.30	Muscle
<i>Synn</i>	Synemin, intermediate filament protein	-1.69	0.31	Muscle
<i>Myh11</i>	Myosin, heavy polypeptide 11, smooth muscle	-1.61	0.33	Muscle
<i>Tpm2</i>	Tropomyosin 2, beta	-1.60	0.33	Muscle
<i>Smtn</i>	Smoothelin	-1.58	0.33	Muscle
<i>Atp2a2</i>	ATPase, Ca ⁺⁺ transporting, cardiac muscle, slow twitch 2	-1.55	0.34	Muscle
<i>Tnnc2</i>	Troponin C2	-1.45	0.37	Muscle contraction and actin binding
<i>Myl4</i>	Myosin light chain 4	-1.30	0.41	Muscle filament sliding and actin filament binding
<i>Myocd</i>	Myocardin	-1.27	0.41	Muscle
<i>Lims2</i>	LIM and senescent cell antigen like domains 2	-1.16	0.45	Muscle
<i>Tpm1</i>	Tropomyosin 1, alpha	-1.06	0.48	Muscle
<i>Lmod1</i>	Leiomodin 1 (smooth muscle)	-1.05	0.48	Muscle
<i>Flna</i>	Filamin, alpha	-1.02	0.49	Muscle
<i>Slimp</i>	Sarcolemma-associated protein	-1.00	0.50	Muscle
<i>Gstm1</i>	Glutathione S-transferase, mu 1	-1.85	0.28	Tumor suppressor and phase II drug metabolism
<i>Fads1</i>	Fatty acid desaturase 1	-1.84	0.28	Tumor suppressor and lipid metabolism
<i>Mrv1</i>	MRV integration site 1	-1.45	0.37	Tumor suppressor
<i>Hspb6</i>	Heat shock protein, alpha-crystallin-related, B6 = HSP20	-1.45	0.37	Tumor suppressor and apoptosis Bax
<i>Pnliprp1</i>	Pancreatic lipase-related protein 1	-1.44	0.37	Tumor suppressor and lipid metabolism
<i>Sdpr</i>	Serum deprivation response	-1.30	0.41	Tumor suppressor and antimetastasis
<i>Gnaz</i>	Guanine nucleotide-binding protein, alpha z subunit	-1.18	0.44	Tumor suppressor
<i>Ras12</i>	RAS-like, family 12	-1.10	0.47	Oncogene-like
<i>Bmp3</i>	Bone morphogenetic protein 3	-1.50	0.35	Cartilage development, cell-cell signaling, development, and differentiation
<i>Ank1</i>	Ankyrin 1, erythroid	-2.08	0.24	Cell shape

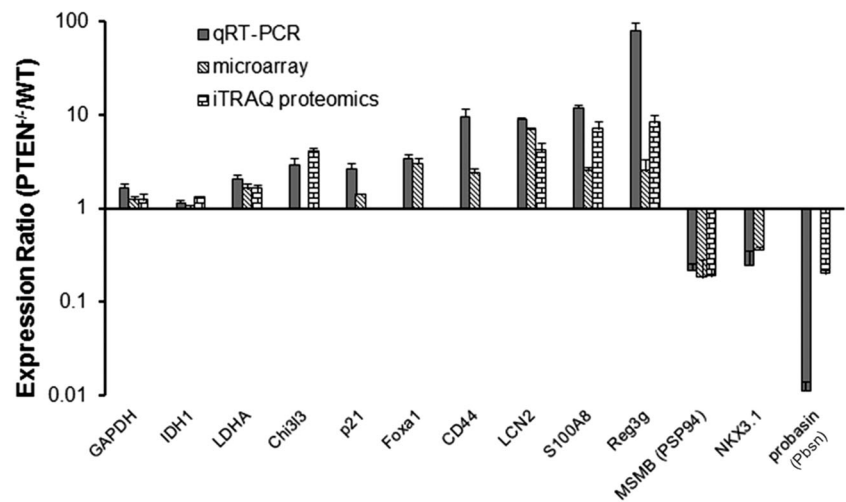
(Continues)

TABLE 2 (Continued)

Genes	Definition	Pten-KO/WT (Log2 FC)	Pten-KO/WT (FC)	Function category
<i>Asb2</i>	Ankyrin repeat and SOCS box-containing 2	-1.16	0.45	Cell shape
<i>Shh</i>	Sonic hedgehog	-1.11	0.46	Cell shape
<i>Arhgef25</i>	Rho guanine nucleotide exchange factor (GEF) 25	-1.00	0.50	Motility
<i>Ckb</i>	Creatine kinase, brain	-1.49	0.36	Extracellular energetics
<i>Smoc1</i>	SPARC related modular calcium binding 1	-0.96	0.51	Calcium ion binding and cell differentiation
<i>Tgm4</i>	Transglutaminase 4 (prostate)	-5.78	0.02	Prostate secretion and androgen regulated
<i>Tagln</i>	Transgelin	-1.58	0.33	Prostate secretion
<i>Akr1b7</i>	Aldo-keto reductase family 1, member B7 = mouse vas deferens protein MVDP	-3.59	0.08	Androgen target gene
<i>Nkx3-1</i>	NK-3 transcription factor, locus 1	-1.46	0.36	Prostate AR target; tumor suppressor
<i>Csrp1</i>	Cysteine and glycine-rich protein 1	-1.26	0.42	Prostate secretion
<i>Cav1</i>	Caveolin 1, caveolae protein	-1.34	0.40	Lipid rafts
<i>Hmgcs2</i>	3-Hydroxy-3-methylglutaryl-coenzyme A synthase 2	-1.28	0.41	Lipogenesis and ketogenic
<i>Prom2</i>	Prominin 2	-1.01	0.50	Cholesterol binding and growth factor activity
<i>Fgl1</i>	Fibrinogen like 1	-0.96	0.51	Adipose tissue development and cholesterol metabolic process
<i>Aqp2</i>	Aquaporin 2	-2.14	0.23	Transporter and water resorption
<i>Slc24a3</i>	Solute carrier family 24 (sodium/potassium/calcium exchanger), member 3	-1.61	0.33	Calcium ion transmembrane transport
<i>Aifm2</i>	Apoptosis-inducing factor, mitochondrion-associated 2	-1.14	0.45	Apoptosis
<i>Depp1</i>	DEPP1 autophagy regulator	-1.01	0.50	Autophagy and regulation of autophagy
<i>Ren1</i>	Renin 1 structural	-1.89	0.27	Mouse-only renin gene
<i>Rnase1</i>	Ribonuclease, RNase A family, 1 (pancreatic)	-1.57	0.34	Anti-inflammation
<i>Rbfox3</i>	RNA binding protein, fox-1 homolog (<i>Caenorhabditis elegans</i>) 3	-1.48	0.36	Neuron marker
<i>Aard</i>	Alanine and arginine rich domain containing protein	-1.05	0.48	Lung development
<i>Nacc2</i>	Nucleus accumbens associated 2, BEN and BTB (POZ) domain containing = RBB	-1.02	0.49	P53 regulator through MDM2
<i>Cd59a</i>	CD59a antigen	-0.98	0.51	Negative regulation of angiogenesis and negative regulation of complement activation

Abbreviations: AR, androgen receptor; FC, fold change; Pten-KO, phosphatase and tensin homolog deleted on chromosome 10-knockout; WT, wild type.

FIGURE 3 Quantitative real-time reverse transcription-polymerase chain reaction (qRT-PCR) detection of mRNA of selected genes/proteins normalized to β -actin for validation of proteomic and microarray platforms. Missing columns were due to either missing hybridization probes (microarray) or lack of protein detection sensitivity by iTRAQ proteomics. iTRAQ, isobaric tags for relative and absolute quantitation; mRNA, messenger RNA



achieve the physical sizes, making predicting PICS from the omics data a challenge.

On the other hand, both proteomic and transcriptomic analyses revealed top molecular signatures related to *immunological diseases and inflammation responses* and predicted involvement of central nodal activities mediated by NF- κ B (Figure 2E). The prediction of NF- κ B signaling was not surprising due to the best-known function of this pathway in inflammation and immune responses. Our observation of greater abundance of myeloid lineage/neutrophil markers calprotectin (S100a8/9) (both omic platforms), lactotransferrin (both omic platforms) and S100a11 (calcizzarin) (Table S7) and Ly6a, Ly6c1, Ly6e, Ly6g6e, and Arg1 (MDSC enriched) and macrophage marker Cd-14 (by microarray, Table 2 and Table S7) in the *Pten*-KO prostate tumors agreed and extended previous study of the Hong Wu laboratory which elaborated the organ-localized endogenous recruitment and expansion of MDSCs and other myeloid lineage granulocytes/neutrophils and monocytes within the *Pten*-KO prostate tumor, conducive for immune suppression and evasion, thereby, promoting cancer progression.²¹ Their conclusion of *Pten*-KO mouse prostate epithelium increased the expression of genes related to the inflammatory and cytokine-to-cytokine signaling network to initiate and expand the immune-suppressive environment²¹ was further strengthened by our microarray detection of overexpression of many cytokines and chemokines and related receptors such as *Il33*, *Cxcl15*, and *Cxcl17* (Table 2) and *Il1b* (also reported by Wu lab), *Il1bc* (interleukin 1 converting enzyme or Caspase 1), *Il12ra1* and *Il1rn* (Table S7).

Comparison with transcriptomics of the Hi-MYC transgenic prostate carcinogenesis model suggested a less prominent involvement of the immune and inflammation signatures in the *Myc* overexpressing mutant prostate in which the cancer was fueled by a different known oncogene (Figure S3, Table S10). Furthermore, in the TRAMP mutant prostate/tumor (Table 1), some of the myeloid/neutrophil marker proteins/genes in *Pten*-KO prostate tumor were not changed (eg, S100a8 and Cfb) or even decreased (eg, Lcn2 and Wfdc2), attesting to a different immune/

inflammatory landscape. The conditional mouse prostate *Pten*-KO model is therefore desirable for studying tumor-relevant immune and inflammation responses to chemopreventive agents or therapeutic modalities.

The most severely suppressed macromolecules reflected diminished *prostate epithelial differentiation* (de-differentiation) in the *Pten*-KO mutant gland in spite of the increased epithelial expansion as reflected by the enriched *chromatin and histone* features. These markers included AR transcriptional targets such as *Pbsn* and *Nkx3.1* (Tables 1 and 2; Figure 3). Their reductions in the *Pten*-KO, TRAMP PIN, and Hi-MYC mutant prostates suggest common cellular features and a possible consequence of carcinogenesis-induced epithelial de-differentiation. Another prominent feature was depressed *muscle* signatures in the *Pten*-KO prostate tumors, which was observed also in other genetically modified carcinogenesis models. One possibility was the changing cellular compositions of the prostate as the epithelial compartment expanded at a faster rate than the smooth muscle compartment. Consistent with this, staining for smooth muscle actin (*Acta2*) in *Pten*-KO or *Myc* driven prostate carcinogenesis models showed loss of continuity of smooth muscle layers surrounding the PIN lesions.^{6,25}

Several unique macromolecules identified by our omic approaches in the *Pten*-KO prostate model are noteworthy for relevance to human PCa biology, diagnostics, prevention, and treatment (Figure 3; Tables 1 and 2). In addition to the preceding discussion of myeloid/neutrophil markers of S100A 8/9 family members, these genes have been reported to be overexpressed in human PCa cells and their ectopic overexpression enhanced infiltration of immune cells, especially neutrophils, and stimulated metastatic seeding of the PCa cells in the lung.²⁷ Regenerating islet-derived protein 3-gamma (Reg3g) has been associated with colonic Paneth cell stemness and survival.²⁸ Two recent studies have revealed a novel immunosuppression role of Reg3g that weakens tumor-specific antigenicity and suppresses antitumor effects of CD8+ T cells in murine models of pancreatic cancer, by activating the JAK2/STAT3 signaling pathway in DCs.^{29,30} Lipocalin-2/NGAL has

been shown to be overexpressed in many solid cancers. In particular, for PCa, its overexpression increased migration and invasion^{31,32}; whereas attenuation of its expression in the PCa cells decreased these processes.^{33,34} Lipocalin-2 was even considered as a screening test for PCa.³⁵ Microsminoprotein- β (MSMB)/Prostate secretory protein of 94 amino acids (PSP94), primarily found in the prostatic secretion, was originally isolated and purified from human seminal plasma. Recent studies have suggested that loss of its expression was associated with PCa aggressiveness.^{36,37}

5 | CONCLUSIONS

Our raw and curated iTRAQ proteomic and microarray transcriptomic data sets of the *Pten*-KO mouse prostate cancer model are available to readers for data mining and interpretation. Our own analyses identified *immune (neutrophil, myeloid lineage, and MDSC) and inflammation responses* as the most profound macromolecular landscape changes, and the involvement of central nodal activities mediated by Akt, NF- κ B, and P53. Consistent with oncogenic transformation were greater *chromatin/histone proliferation features* and more *ion and nutrient transporters* in the *Pten*-KO prostate. Other alterations involved suppressed *prostate differentiation, smooth muscle features, ER stress responses*, and altered *glutathione and antioxidant functions*. These macromolecular alterations suggest likely changes in anabolic intermediate metabolites and cellular energy metabolism. Such questions will be addressed in a separate paper with a metabolomic profiling approach and integrative bioinformatics analyses of multiple omics data sets.

ACKNOWLEDGMENTS

The authors thank Kay Gurley at Fred Hutchinson Cancer Research Center for bio-specimens management; LeeAnn Higgins, PhD and Todd Markowski at University of Minnesota for peptide fractionation and proteomic analysis; Jerry Daniel at University of Minnesota for microarray analysis; Su-Ni Tang, PhD at Texas Tech University Health Sciences Center for help on tissue processing. The authors also thank Jiangang Liao, PhD, director of the Penn State Cancer Institute Biostatistics core for statistical advice; and Yuka Imamura, PhD, director of Genome Sciences core for guidance on bioinformatics. This study has been supported, in part, by R01CA172169 grant from US National Cancer Institute, Texas Tech University Health Sciences Center Preliminary Data Grant (to JZ) and Penn State College of Medicine Start-up fund (to JL).

CONFLICTS OF INTEREST

The authors declare that there are no conflicts of interest.

DATA AVAILABILITY STATEMENT

Data that supports the findings of this study are available in the supplementary materials of this article.

ORCID

Junxuan Lü  <http://orcid.org/0000-0002-2354-7186>

REFERENCES

1. Siegel RL, Miller KD, Jemal A. Cancer statistics, 2019. *CA Cancer J Clin*. 2019;69(1):7-34.
2. Song MS, Salmena L, Pandolfi PP. The functions and regulation of the PTEN tumour suppressor. *Nat Rev Mol Cell Biol*. 2012;13(5):283-296.
3. Han B, Mehra R, Lonigro RJ, et al. Fluorescence in situ hybridization study shows association of PTEN deletion with ERG rearrangement during prostate cancer progression. *Mod Pathol*. 2009;22(8):1083-1093.
4. Yoshimoto M, Cutz JC, Nuin PAS, et al. Interphase FISH analysis of PTEN in histologic sections shows genomic deletions in 68% of primary prostate cancer and 23% of high-grade prostatic intra-epithelial neoplasias. *Cancer Genet Cytogenet*. 2006;169(2):128-137.
5. Whang YE, Wu X, Suzuki H, et al. Inactivation of the tumor suppressor PTEN/MMAC1 in advanced human prostate cancer through loss of expression. *Proc Natl Acad Sci U S A*. 1998;95(9):5246-5250.
6. Wang S, Gao J, Lei Q, et al. Prostate-specific deletion of the murine *Pten* tumor suppressor gene leads to metastatic prostate cancer. *Cancer Cell*. 2003;4(3):209-221.
7. Greenberg NM, DeMayo F, Finegold MJ, et al. Prostate cancer in a transgenic mouse. *Proc Natl Acad Sci U S A*. 1995;92(8):3439-3443.
8. Chakraborty S, Hosen MI, Ahmed M, Shekhar HU. Onco-multi-OMICs approach: a new frontier in cancer research. *BioMed Res Int*. 2018;2018:9836256.
9. Cima I, Schiess R, Wild P, et al. Cancer genetics-guided discovery of serum biomarker signatures for diagnosis and prognosis of prostate cancer. *Proc Natl Acad Sci U S A*. 2011;108(8):3342-3347.
10. Kelly-Spratt KS, Kasarda AE, Igra M, Kemp CJ. A mouse model repository for cancer biomarker discovery. *J Proteome Res*. 2008;7(8):3613-3618.
11. Zhang J, Wang L, Anderson LB, Witthuhn B, Xu Y, Lu J. Proteomic profiling of potential molecular targets of methyl-selenium compounds in the transgenic adenocarcinoma of mouse prostate model. *Cancer Prev Res (Phila)*. 2010;3(8):994-1006.
12. Zhang J, Wang L, Zhang Y, Li L, Higgins L, Lu J. Lobe-specific proteome changes in the dorsal-lateral and ventral prostate of TRAMP mice versus wild-type mice. *Proteomics*. 2011;11(12):2542-2549.
13. Zhang J, Wang L, Zhang Y, et al. Chemopreventive effect of Korean Angelica root extract on TRAMP carcinogenesis and integrative "omic" profiling of affected neuroendocrine carcinomas. *Mol Carcinog*. 2015;54(12):1567-1583.
14. Lin-Moshier Y, Sebastian PJ, Higgins L, Sampson ND, Hewitt JE, Marchant JS. Re-evaluation of the role of calcium homeostasis endoplasmic reticulum protein (CHERP) in cellular calcium signaling. *J Biol Chem*. 2013;288(1):355-367.
15. Shukla S, Shankavaram UT, Nguyen P, Stanley BA, Smart DK. Radiation-induced alteration of the brain proteome: understanding the role of the sirtuin 2 deacetylase in a murine model. *J Proteome Res*. 2015;14(10):4104-4117.
16. Mallawaarachy DM, Buckland ME, McDonald KL, et al. Membrane proteome analysis of glioblastoma cell invasion. *J Neuropathol Exp Neurol*. 2015;74(5):425-441.
17. Kovacic B, Hoelbl-Kovacic A, Fischhuber KM, et al. Lactotransferrin-Cre reporter mice trace neutrophils, monocytes/macrophages and distinct subtypes of dendritic cells. *Haematologica*. 2014;99(6):1006-1015.
18. Chen Z, Trotman LC, Shaffer D, et al. Crucial role of p53-dependent cellular senescence in suppression of *Pten*-deficient tumorigenesis. *Nature*. 2005;436(7051):725-730.
19. Wang L, Guo X, Wang J, et al. Methylseleninic acid superactivates p53-senescence cancer progression barrier in prostate lesions of *Pten*-knockout mouse. *Cancer Prev Res (Phila)*. 2016;9(1):35-42.

20. Alimonti A, Nardella C, Chen Z, et al. A novel type of cellular senescence that can be enhanced in mouse models and human tumor xenografts to suppress prostate tumorigenesis. *J Clin Invest*. 2010;120(3):681-693.
21. Garcia AJ, Ruscetti M, Arenzana TL, et al. Pten null prostate epithelium promotes localized myeloid-derived suppressor cell expansion and immune suppression during tumor initiation and progression. *Mol Cell Biol*. 2014;34(11):2017-2028.
22. Bezzi M, Seitzer N, Ishikawa T, et al. Diverse genetic-driven immune landscapes dictate tumor progression through distinct mechanisms. *Nat Med*. 2018;24(2):165-175.
23. Di Mitri D, Toso A, Chen JJ, et al. Tumour-infiltrating Gr-1+ myeloid cells antagonize senescence in cancer. *Nature*. 2014;515(7525):134-137.
24. Jung SH, Hwang HJ, Kang D, et al. mTOR kinase leads to PTEN-loss-induced cellular senescence by phosphorylating p53. *Oncogene*. 2019;38(10):1639-1650.
25. Ellwood-Yen K, Graeber TG, Wongvipat J, et al. Myc-driven murine prostate cancer shares molecular features with human prostate tumors. *Cancer Cell*. 2003;4(3):223-238.
26. Vivanco I, Palaskas N, Tran C, et al. Identification of the JNK signaling pathway as a functional target of the tumor suppressor PTEN. *Cancer Cell*. 2007;11(6):555-569.
27. Grebhardt S, Muller-Decker K, Bestvater F, Hershinkel M, Mayer D. Impact of S100A8/A9 expression on prostate cancer progression in vitro and in vivo. *J Cell Physiol*. 2014;229(5):661-671.
28. Zhao D, Kim YH, Jeong S, et al. Survival signal REG3alpha prevents crypt apoptosis to control acute gastrointestinal graft-versus-host disease. *J Clin Invest*. 2018;128(11):4970-4979.
29. Yin G, Du J, Cao H, Liu X, Xu Q, Xiang M. Reg3g promotes pancreatic carcinogenesis in a murine model of chronic pancreatitis. *Dig Dis Sci*. 2015;60(12):3656-3668.
30. Liu X, Zhou Z, Cheng Q, et al. Acceleration of pancreatic tumorigenesis under immunosuppressive microenvironment induced by Reg3g overexpression. *Cell Death Dis*. 2017;8(9):e3033.
31. Ding G, Fang J, Tong S, et al. Over-expression of lipocalin 2 promotes cell migration and invasion through activating ERK signaling to increase SLUG expression in prostate cancer. *Prostate*. 2015;75(9):957-968.
32. Ding G, Wang J, Feng C, Jiang H, Xu J, Ding Q. Lipocalin 2 over-expression facilitates progress of castration-resistant prostate cancer via improving androgen receptor transcriptional activity. *Oncotarget*. 2016;7(39):64309-64317.
33. Tung MC, Hsieh SC, Yang SF, et al. Knockdown of lipocalin-2 suppresses the growth and invasion of prostate cancer cells. *Prostate*. 2013;73(12):1281-1290.
34. Rahimi S, Roushandeh AM, Ebrahimi A, Samadani AA, Kuwahara Y, Roudkenar MH. CRISPR/Cas9-mediated knockout of Lcn2 effectively enhanced CDDP-induced apoptosis and reduced cell migration capacity of PC3 cells. *Life Sci*. 2019;231:116586.
35. Muslu N, Ercan B, Akbayir S, Balci S, Ovla HD, Bozlu M. Neutrophil gelatinase-associated lipocalin as a screening test in prostate cancer. *Turk J Urol*. 2017;43(1):30-35.
36. Andreas ML, Ali AT, Jan M, et al. Loss of PSP94 expression is associated with early PSA recurrence and deteriorates outcome of PTEN deleted prostate cancers. *Cancer Biol Med*. 2019;16(2):319-330.
37. Bergstrom SH, Jaremo H, Nilsson M, Adamo HH, Bergh A. Prostate tumors downregulate microseminoprotein-beta (MSMB) in the surrounding benign prostate epithelium and this response is associated with tumor aggressiveness. *Prostate*. 2018;78(4):257-265.

SUPPORTING INFORMATION

Additional supporting information may be found online in the Supporting Information section.

How to cite this article: Zhang J, Kim S, Li L, Kemp CJ, Jiang C, Lü J. Proteomic and transcriptomic profiling of *Pten* gene-knockout mouse model of prostate cancer. *The Prostate*. 2020;80:588-605. <https://doi.org/10.1002/pros.23972>